NANO LETTERS

Letter

pubs.acs.org/NanoLett

Terms of Use CC-BY

Straining Graphene Using Thin Film Shrinkage Methods

Hiroki Shioya,*[,†] Monica F. Craciun,[‡] Saverio Russo,[‡] Michihisa Yamamoto,[†] and Seigo Tarucha[†,§]

[†]Department of Applied Physics, University of Tokyo, Tokyo, Japan

[‡]Center for Graphene Science, CEMPS, University of Exeter, Devon EX4, United Kingdom

[§]Center for Emergent Matter Science (CEMS), RIKEN, Wako, Saitama, Japan

ABSTRACT: Theoretical works suggest the possibility and usefulness of strain engineering of graphene by predicting remarkable properties, such as Dirac cone merging, bandgap opening and pseudo magnetic field generation. However, most of these predictions have not yet been confirmed because it is experimentally difficult to control the magnitude and type (e.g., uniaxial, biaxial, and so forth) of strain in graphene devices. Here we report two novel methods to apply strain without bending the substrate. We employ thin films of evaporated metal and organic insulator deposited on graphene, which shrink after electron beam irradiation or heat application. These methods make it possible to apply both biaxial strain and in-plane isotropic compressive strain in a well-controlled manner. Raman spectroscopy measurements show a clear splitting of the degenerate states of the G-band in the case of biaxial strain, and G-band blue shift without splitting in the case of in-plane isotropic compressive strain. In the case of biaxial strain application, we find out the ratio of the strain component perpendicular to the stretching direction is at least three times larger than what was previously observed, indicating that shrinkage of the metal or organic insulator deposited on graphene induces both tensile and compressive strain in this atomically thin material. Our studies present for the first time a viable way to apply strain to graphene without the need to bend the substrate.

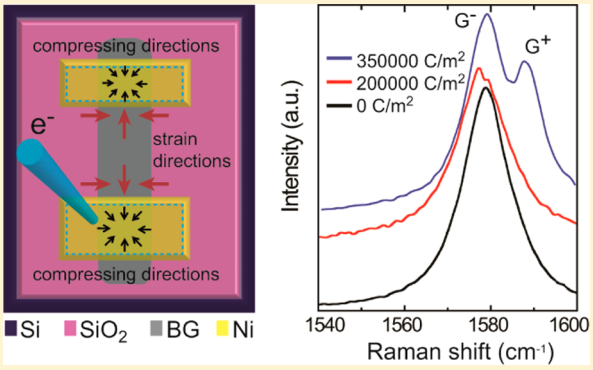

KEYWORDS: *Graphene, planar process, shrinkage of thin films, tensile and compressive strain, Raman spectrum, strain engineering of two-dimensional crystals*

Since its discovery, graphene[1,2] has attracted growing interest due to the unique array of physical properties, which characterizes this material. This single layer of carbon atoms is expected to enable the development of conceptually new electronic devices as already indicated by recent feasibility studies.[3−8] For example, the unique relation between the crystal structure of graphene and its energy dispersion could be used to control strain-induced pseudo magnetic fields[9] and a strain-induced bandgap.[10−12] In particular, it has been theoretically predicted that when strain is applied along the three main crystallographic directions of graphene, a large pseudo magnetic field is generated. The magnitude of the pseudo magnetic field is expected to be 40T for 10% strain.[9] This should lead to observable changes in the electrical transport properties of graphene, such as quantization of the conductance due to the creation of strain-induced pseudo magnetic field in which Landau levels are formed without external magnetic field. Furthermore, a uniaxial strain of more than 20% applied along the zigzag direction is expected to drive the merging of Dirac cones and the opening of a bandgap in the energy dispersion of graphene.[10−12] Strain engineering in graphene combined exploiting the possibility to guide electrons in graphene devices by internally generated pseudo magnetic fields is at the core of novel multifunctional electric applications.[13]

Signatures of strain-induced pseudo magnetic fields have been reported very recently by scanning tunneling microscopy studies in graphene nanobubbles.[14,15] Changes in the electrical transport properties of strained graphene on flexible substrates have also been reported in several experimental studies.[16−22] Furthermore, controlled tensile and compressive uniaxial strain has been demonstrated by bending a flexible substrate onto which graphene was deposited.[23−25] Raman spectroscopy was successfully used as a tool to monitor the strain, since both the G and 2D peaks of graphene are sensitive to strain. Specifically, the G peak originates from a first order Raman scattering process, which corresponds to the doubly degenerate E_{2g} phonon at the center of the Brillouin zone (BZ), whereas the 2D peak arises from a second-order double-resonant process between the K and K′ points in the BZ involving two zone-boundary phonons.[26] Both the G and 2D peaks of graphene show (1) a red shift under tensile strain due to phonon softening and (2) a blue shift upon compression due to phonon hardening.[25] In addition, as the magnitude of uniaxial strain increases or the anisotropy in graphene increases, these Raman

Received: October 2, 2013
Revised: January 8, 2014
Published: February 3, 2014

 © 2014 American Chemical Society

peaks split into two subpeaks, which correspond to symmetry breakings of the degenerate phonon modes.[24] To date the only experimental method demonstrating a control of strain in graphene requires bending the substrate and this technique only allows a limited control over the direction of strain that can be engineered in the transistors on the substrate. Indeed with this technique it is very difficult to engineer a strain configuration in graphene that is not uniaxial, such as that required to generate uniform pseudomagnetic fields or required to open a bandgap. In addition, since the curvature of the bending substrate is not uniform over large areas, for example, wafer scale, this technique is not suitable for the integration of many devices.

Here, we demonstrate two different methods to control strain in graphene using the effect of recrystallization of metallic films, and condensation polymerization of organic insulating films, attached to the graphene, respectively. Neither method requires substrate bending. Control over the recrystallization of the metal films and the condensation polymerized regions of the organic films enables engineering of more complex strain in flat structures of graphene devices. Moreover, our methods allow fabrication of a large number of strained devices on the same substrate with the area and magnitude of the strain tunable for each strained device.

Metallic contact electrodes to graphene are typically formed by evaporated metal thin films, which have an amorphous crystal structure. When the metallic contacts are recrystallized, for example, by supplying sufficiently high energy, there appears a change in the density of the films that causes a compressive strain in the graphene under the contacts. Consequently, the graphene between the two contacts is laterally strained by a stretching force directed along the line of the two contacts and by a compressing force in the transverse direction (see Figure 1a). Therefore, control over the recrystallization of the contact metal can offer a direct way to engineer strain patterns in graphene depending on the layout of the contacts.

Organic insulating films, which are usually used in large scale integrations (LSIs) as an interlayer dielectric, shrink when exposed to an electron-beam or upon thermal annealing at such a high level that condensation polymerization of the films occur.[27] When these films are deposited on graphene, shrinkage of the films can be used to introduce strain in this atomically thin material. Therefore, by controlling locally the condensation polymerization of the organic films it should be possible to engineer biaxial strain or homogeneous compressive strain, which have been notoriously difficult to attain experimentally.

To date the recrystallization of the metal contacts and the condensation polymerization of the organic films as means to control strain in graphene have not yet been explored. Here we show the potential of this novel technology for engineering strain patterns.

In the analyses of biaxial strain, we focus on the effect of isotropic compression driven by the shrinkage (recrystallization and condensation polymerization) of graphene covered by the metal or the organic insulating layer. This effect can enhance anisotropy of the strained states compared with the methods using flexible substrates.

The applied strain is evaluated by Raman spectroscopy, using RM 1000 (Renishaw) and NRS-1000 (JASCO corp.) with the excitation wavelength of 532 nm. The grating is 2400 grooves/mm for RM 1000 and 1800 grooves/mm for NRS-1000. The diameter of the probing spot is between two to three

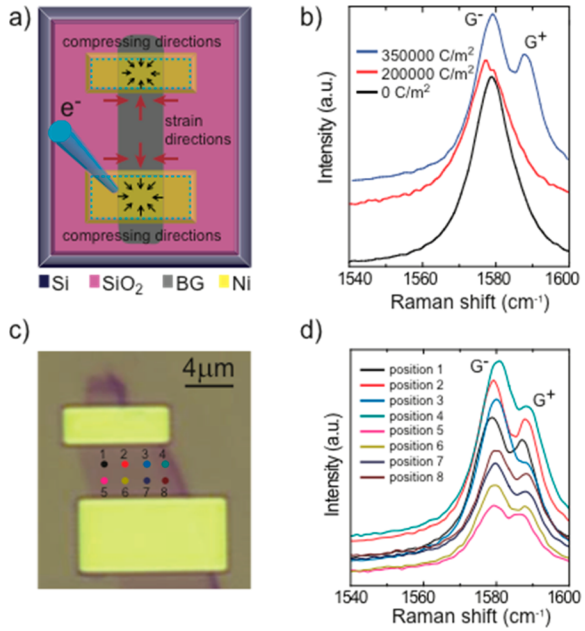

Figure 1. (a) Schematic diagram for applying biaxial strain on bilayer graphene by electron beam irradiation on the metal thin films (yellow rectangles). Electron beam irradiation inside the blue rectangle region induces strain on graphene (gray region) along the direction of the red arrows. (b) Electron beam dose dependence of the G-band peak of the Raman spectrum. Clear G-band peak splitting represents the presence of biaxial strain. The definition of the G^+ and G^- peaks follows the ref 24. (c) Optical micrograph of the sample. Raman spectra are measured at each colored position labeled 1−8. (d) Raman spectra measured at the positions indicated in (c). The small variety of the applied strain is confirmed.

micrometers and the spectral resolution is approximately 1 cm^{-1} for both RM 1000 and NRS-1000.

To analyze the degree of the applied strain, we adopt a well-established model in which the shift of the G-band peak carries the information of the strain present in graphene.[24] The key aspects of this model are captured by the following equation

$$\Delta\omega_{E2g}{}^{\pm} = -\omega_{E2g}{}^{0}\gamma_{E2g}(\varepsilon_{ll} + \varepsilon_{tt}) \pm \frac{1}{2}\beta_{E2g}\omega_{E2g}{}^{0}(\varepsilon_{ll} - \varepsilon_{tt}) \quad (1)$$

in which ε_{ll} (ε_{tt}) is the parallel (perpendicular) strain component to the applied strain whose positive (negative) value means tension (compression) for a given Grueneisen parameter $\gamma = 1.99$,[28] a shear deformation potential $\beta = 0.99$,[28] the wavenumber ω^0 at G-band peak without strain, and the experimentally measured shift $\Delta\omega$ of the wavenumber at G-band due to the strain from the state without strain.

The biaxial strain introduces anisotropy in what are initially two degenerate oscillation modes of the graphene sublattices contributing to a single peak of the G-band, so that the Raman spectrum of the G-band is decomposed into two Lorentzian peaks indicated by G^+ and G^-. From the shifts of $\Delta\omega_{E2g}{}^{\pm}$ of these peaks, the degree of the strain can be evaluated.[24]

In the metal recrystallization method, we control biaxial strain between two thin film contacts of Nickel (Ni) (around 20 nm thick) evaporated directly on mono- and bilayer graphene flakes. Recrystallization of the Ni films is induced by irradiation of these with an electron beam (Figure 1a). The separation between the Ni contacts is 4.5 μm as shown in Figure 1c, which is larger than the spot size of the laser beam in

dx.doi.org/10.1021/nl403679f | Nano Lett. 2014, 14, 1158−1163

our Raman spectroscopy system. Figure 1b shows the Raman spectra of a bilayer graphene placed between two Ni film contacts before and after electron beam irradiation-induced recrystallization. It is clear that the G-band peak splits upon electron beam irradiation of Ni. In particular, we find that the higher is the electron beam dose, the larger is the G-band peak splitting. This result shows that the degree of strain in the graphene flake is controllable as a function of electron beam dose.

In the higher dose case of 350 000 C/m^2 the G^+ peak position is shifted to higher energy (blue shifted) indicating compression, while the G^- peak shows red shift in the lower dose case of 200 000 C/m^2. To address this difference, we need to analyze the strain components. By applying eq 1 to the lower dose case, we obtained $(\varepsilon_{ll}, \varepsilon_{tt}) = (0.093, -0.015)$ (%) with the ratio $|\varepsilon_{tt}/\varepsilon_{ll}|$ of 0.161. The small strain components indicate that the magnitude of the strain is relatively small. The ratio $|\varepsilon_{tt}/\varepsilon_{ll}|$ of 0.161 is comparable to the Poisson's ratio = 0.186 of pristine graphene derived by the first principle calculation.[28] It is apparent from the definition of the Poisson's ratio that the graphene flake is only slightly pulled by the two contacts along the vertical direction of Figure 1a without being compressed externally along its perpendicular direction, that is, the vertical tensile force is much more efficient than the horizontal compressive force in this case. This is maybe related to the direction of tension or compression. In this lower dose case, the effect of tension along the line of two contacts can be higher than that of compression along the perpendicular direction to that line. The situation becomes different when a higher dose, corresponding to 350 000 C/m^2, is applied to get closer to the saturation of the recrystallization process of the Ni film. In this case, the evaluated strain components (%) are $(\varepsilon_{ll}, \varepsilon_{tt}) = (0.26, -0.38)$ with the ratio $|\varepsilon_{tt}/\varepsilon_{ll}|$ of 1.46, which is about 8 times larger than the value of 0.186. The enhancement of negative ε_{tt} indicates additional compression via shrinkage of contact metals along the horizontal arrows in Figure 1a. This experimental finding provides direct evidence that the electron beam irradiation causes shrinkage of the evaporated Ni films, resulting in a tensile strain with $\varepsilon_{ll} > 0$ and a compressive strain $\varepsilon_{tt} < 0$ in the graphene (See Figure 1a). This is also consistent with the observation of the large blue shift of the G^+ band peak Raman spectrum observed upon irradiating with 350 000 C/m^2 since blue shift of this Raman peak occurs in the presence of the compressive strain.

To examine the spatial distribution or uniformity of the strain in graphene we measure the Raman spectra at eight different locations on the flake as indicated in Figure 1c after exposing the Ni metal contacts to 350 000 C/m^2. The Raman spectra at each of the forementioned locations show a similar trend: the G-peak splits and shifts (see Figure 1d). The standard deviation (σ) of the strain components (ε_{ll}, ε_{tt}) are $\sigma_{ll} = 0.0175$ for ε_{ll} and $\sigma_{tt} = 0.020$ for ε_{tt}, and the average values are $\langle\varepsilon_{ll}\rangle = 0.275$ and $\langle\varepsilon_{tt}\rangle = -0.376$. These indicate that 96% (2σ) of the strained region has deviation of less than 12.8% of $\langle\varepsilon_{ll}\rangle$ and less than 10.6% of $\langle\varepsilon_{tt}\rangle$. We therefore conclude that the strain distribution is close to uniform over 5 (horizontal direction) × 3 (vertical direction) μm^2.

The evaporated metal shrinkage method is also applied to a monolayer graphene to induce biaxial strain. An AFM image of the monolayer sample is shown in Figure 2a. The distance between the two metallic contacts is 3 μm. The G-band Raman spectra of monolayer graphene before and after electron beam irradiation with the dose of 64 000 C/m^2 are shown in Figure 2b. The evaluated strain components (%) are $(\varepsilon_{ll}, \varepsilon_{tt}) = (0.38, -0.26)$ with the ratio $|\varepsilon_{tt}/\varepsilon_{ll}|$ of 0.68. This ratio is more than 3.5 times higher than the Poisson's ratio of pristine graphene.[28] The ratio is smaller than that of the obtained with the bilayer graphene upon irradiating with a dose of 350 000 C/m^2 but larger than that for the dose of 200 000 C/m^2. We did not go into the higher dose with the monolayer sample because we found experimentally that the Ni contacts are easily removed from the substrate upon irradiating with the high dose especially when the size of the contacts is relatively small. The higher ratio $|\varepsilon_{tt}/\varepsilon_{ll}|$ of bilayer graphene shows a higher blue shift of G^+ peak and this is consistent with higher compression. In this comparison, we infer that the difference of their dose conditions may be causing a discrepancy in the realized strain.

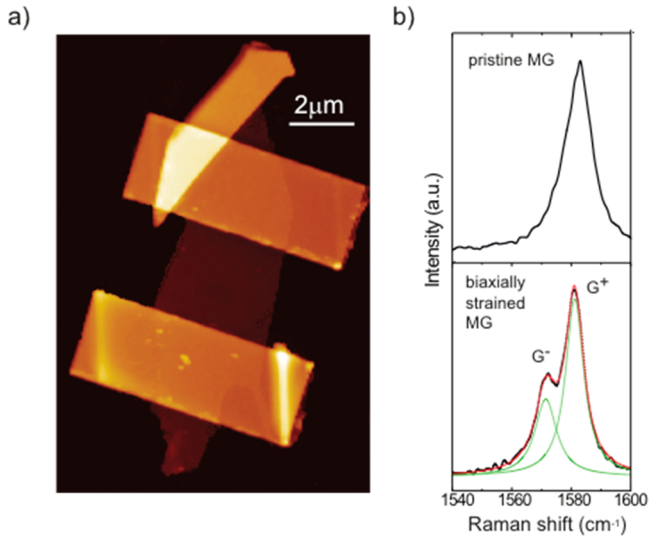

Figure 2. (a) AFM image of the monolayer graphene sample after electron beam irradiation. The monolayer graphene flake is set at the center of this image and the two rectangles on the flake are evaporated Ni contacts. (b) Raman spectra of the monolayer graphene shown in (a). The upper (lower) panel shows the spectrum measured before (after) electron beam irradiation. A clear G-band peak splitting, which is decomposed into two Lorentzian peaks (green curves), is observed in the lower panel.

In general, parameters that characterize the strain include the size and thickness of graphene flakes, the geometry of the contacts, the distance between the metal contacts, and the electron beam irradiation dose. Among these parameters, the separation between the contacts is one of the most effective and easy to control experimentally. By designing the contact geometries, we can in principle arbitrarily design and tune the strain.

After electron beam irradiation of 350 000 C/m^2, the bilayer flake is stretched by 0.26% along the longitudinal direction that connects the two contacts. This with the contact separation of 4.5 μm leads to 11.7 nm prolongation of the bilayer graphene. Hence, by reducing the separation d between the Ni contacts it is possible to induce much larger strain. For example, if d = 100(30) nm, the degree of strain should be 11.7(39)%. On the other hand, an upper limit of the stretching graphene is determined by the mechanical failure of this atomically thin material found to be 12% in previous experiments.[29]

Our method should allow for inducing strain more than 10% without the need for bending the substrate. The large values of strain that can be engineered using this method are comparable to the required values needed to access novel physical regimes.

dx.doi.org/10.1021/nl403679f | Nano Lett. 2014, 14, 1158−1163

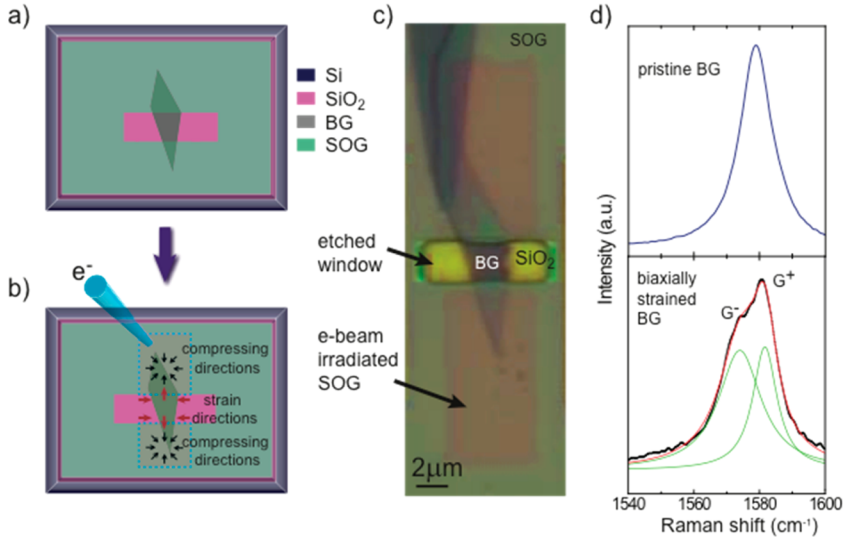

Figure 3. (a) Schematic diagram of the sample in which biaxial strain is applied with the SOG material (before electron beam irradiation). The SOG material was first coated on the entire sample surface and the center part in pink was then etched for the efficient strain application in the next step. (b) Schematic representation of electron beam irradiation. The electron beam was irradiated inside the two blue rectangle regions to induce strain in graphene along the direction indicated by the red arrows. (c) Optical micrograph of a sample as schematically shown in panel b. (d) Raman spectra of the G-band peak of bilayer graphene before and after the strain application using the SOG material. The upper panel shows the G-band peak of pristine bilayer graphene and the lower panel shows that with biaxial strain: black curve for the raw data and red curve for the fitting with superposition of two Lorentzian curves in green. Biaxially strained bilayer graphene by the SOG material also shows the G-peak splitting.

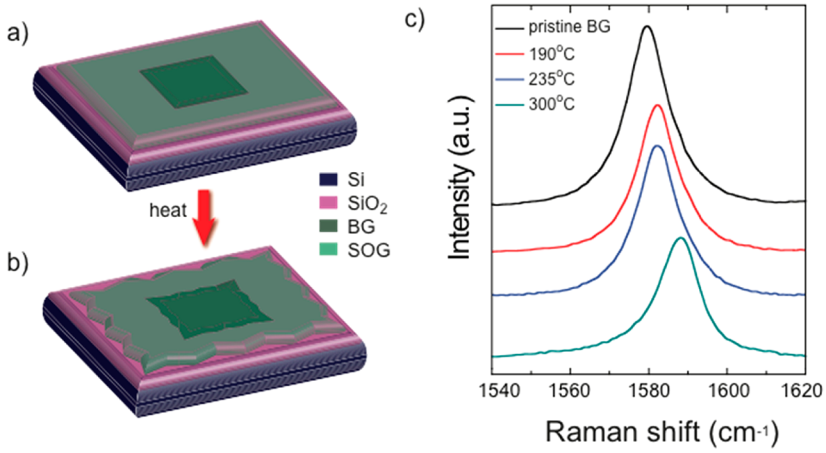

Figure 4. (a) Schematics of the sample structure before application of isotropic compressive strain. The SOG material is coated on the entire surface. (b) Schematics of the sample after application of isotropic compressive strain. After heat treatment, the SOG layer shrinks by condensation polymerization and a compressive strain is induced in graphene covered by the SOG film. (c) The G-band peak of the Raman spectrum for different degrees of isotropic-compressive strain in the bilayer graphene induced by baking at different temperatures. As the temperature increases, the peak position shifts to the higher energy. This explains that the compressive strain is applied on graphene underneath the shrunken SOG film.

For example, Guinea et al.[9] predicts that 10% of strain will induce 40T of the pseudo magnetic field while Guinea[30] predicts 1% of strain will induce more than 1T of the field. Our methods would also enable to stretch graphene along the zigzag axis over 20% by putting the contacts along the zigzag direction with a narrow gap if the in-plane failure strength is over 20%, Dirac cone merging[10−12] could then be observed.

Finally previous studies have shown that charge-doping graphene can also lead to a blue shift of the G-band Raman peak.[31,32] More specifically, ref 32 explains that the doping effect by amorphous carbon materials affected by electron beam irradiation in the vacuum chamber causes a blue shift. However, we exclude that the observed blue shift of the G-band Raman peak in our experiments is due to charge doping because we take care to do not irradiate with electrons directly graphene but only the materials (Ni and organic films) deposited on graphene. Furthermore we can also exclude that a possible change in the doping of graphene, which may arise from the proximity exposure of the electron beam irradiation onto the nearby Ni electrodes, plays any significant role in our experiments. This is demonstrated by the fact that we measure the Raman spectra of pristine graphene without any apparent blue shift of the G-peak after irradiating the Ni film to such high dose that it is removed from the substrate. Finally, the consistency between the evaluated ratios of $|\varepsilon_{tt}/\varepsilon_{ll}|$ and the higher peak positions is yet another indication that the observed G-band blue shift is driven by strain.

In the second method, spin on glass (SOG) material is spin coated on bilayer graphene flakes. A biaxial strain is applied efficiently by etching a window in the SOG material in the

dx.doi.org/10.1021/nl403679f | Nano Lett. 2014, 14, 1158−1163

center of the graphene flake (see Figure 3a) and by driving the polymerization with electron beam irradiation at doses higher than 50000 C/m^2 (see Figure 3b,c). In addition, we use thermal annealing (from 190 to 300 °C in atmospheric condition) to introduce an isotropic compressive strain in graphene uniformly coated by the SOG film. In both cases, that is, electron irradiation and thermal annealing, we find experimentally that the contact force between graphene and SOG is high enough to apply a load to graphene. Here, we present the study of the Raman G-band spectra of bilayer graphene samples. More specifically, upon applying biaxial strain the G-peak is decomposed into two peaks, see Figure 3d. The strain components evaluated from this result are (ε_{ll}, ε_{tt}) = (0.29, −0.22) with $|\varepsilon_{tt}/\varepsilon_{ll}|$ = 0.76. This ratio is more than 4 times larger than the Poisson's ratio of pristine graphene evaluated by the first principle calculation.[28] This experimental finding is consistent with the shrinkage of the SOG layer affected by condensation polymerization. Furthermore, the ratio of ε_{tt} is higher than the case of a pristine graphene, which is similar to what we observe upon engineering strain in graphene by electron beam irradiating Ni contacts. Therefore, shrinking SOG by condensation polymerization and shrinking the Ni metal by recrystallization are two independent methods to engineer strain in graphene.

We now proceed to analyze an independent way to introduce strain in graphene based on spin coating the entire surface of the devices with SOG, see Figure 4a,b. In this case, the degree of condensation polymerization is controlled by varying the annealing temperature and consequently we control the degree of strain in graphene. Figure 4c shows the measured G-band Raman spectra before annealing and after annealing at 190, 235, and 300 °C in atmospheric conditions. As the annealing temperature increases, the G-band Raman peak shifts to high energy (blue shift). This reflects the increased elastic energy of graphene due to the compressive strain. Because the isotropic shrinkage of the SOG film does not break symmetry of the honeycomb lattice, the G-band peak does not split.

In this case, the applied strain is evaluated from the shift $\Delta\omega_{E2g}$ of the G-band peak measured from that of the pristine graphene, using the following equation[24]

$$\Delta\omega_{E2g} = -2\omega_{E2g}{}^{0}\gamma_{E2g}\varepsilon \tag{2}$$

This equation is derived by replacing ε_{ll} and ε_{tt} with ε in eq 1. Then from the observed $\Delta\omega_{E2g}$, we obtain ε = 0.16% after annealing at of 300 °C. This compressive feature is consistent with the effect of shrinkage from condensation polymerization of SOG material.

Finally, to assess the goodness of the Ni metal and SOG methods for engineering large strain in graphene we compare the ratio $|\varepsilon_{tt}/\varepsilon_{ll}|$ for biaxially strained graphene determined in our experiments with the values reported in previous studies, see Table 1. In all cases, we find $|\varepsilon_{tt}/\varepsilon_{ll}|$ which is at least a factor of 2 higher than previously achieved upon curvature-induced strain due to substrate bending.[24] In particular, in the case of bilayer graphene strained by the recrystallized Ni film we find a record high value of $|\varepsilon_{tt}/\varepsilon_{ll}|$ equal to 1.53. Such high values of $|\varepsilon_{tt}/\varepsilon_{ll}|$ can be accomplished with our method owing to the isotropic shrinkage of the thin film materials attached to graphene. In this case, compression by the thin film shrinkage deposited on graphene in addition to the shrinkage of graphene itself as explained by Poisson's ratio generates higher ratios of $|\varepsilon_{tt}/\varepsilon_{ll}|$ ranging from 0.68 to 1.53 as demonstrated in our study.

Table 1. Comparison of the Ratio $|\varepsilon_{tt}/\varepsilon_{ll}|$ for Biaxally Strained Graphene Determined in This Study with Values Reported in Previous Studies

	the ratio $|\varepsilon_{tt}/\varepsilon_{ll}|$
PRB 79, 205433 (2009) [ref 24]	0.33 (the value of the adhesion layer)
ACS Nano 2, 2301 (2008) [ref 23]	0.186 (first principle calculation of graphene)
this study (Ni film) bilayer graphene	1.53 (mean value of 8 points)
this study (Ni film) monolayer graphene	0.68
this study (SOG) bilayer graphene	0.76

Shrinkage in our methods enhances the role played by ε_{tt} in increasing the ratio $|\varepsilon_{tt}/\varepsilon_{ll}|$.

In conclusion, two different methods for engineering strain in graphene were demonstrated employing the shrinkage property of thin films placed on graphene in a planar geometry without the need for bending the substrate. Both biaxial strained states and isotropic compressive strained states of graphene were achieved in a controlled manner. The realized strain shows small variety or almost uniform strained states anywhere on the substrate paving the way to integrate strained graphene devices on planar chips. The shrinkage property of the thin films brings a high ratio $|\varepsilon_{tt}/\varepsilon_{ll}|$, which is enhanced by a compressive force applied on the area of graphene between the thin film contacts. The methods demonstrated in this study hold the promise for the development of strain engineering of graphene and help explore novel physics in strained graphene. Moreover, the present technique is general enough such that it can be applied to other two-dimensional crystals, such as atomically thin metal dichalcogenides.

Methods. *Sample Preparation.* In the sample preparation, heavily p-doped Si substrate with a thermally oxidized layer (SiO_2 layer) of 285 nm thickness on top is employed. First, a small metallic pattern is deposited on the SiO_2 substrates used as alignment markers between graphene flakes. Graphene flakes are then exfoliated mechanically from a graphite piece and printed on the substrate. The number of layers of graphene is identified from measurement of the green light intensity[33] and the 2D-band of Raman spectra.[34] Then, for the metal thin film method, Ni films are deposited by an electron beam evaporator. Or for the SOG method an SOG material (Accuglass T-11 (211), Honeywell Corp.) is deposited on graphene by spin coating at 3000 rpm for 40 s followed by baking to form a cross-linked structure of organic materials. The resultant thickness of SOG is 200 nm. The metal markers, Ni films, and the SOG materials are patterned by electron beam lithography (Elionix 7700 system) using the electron beam resist NANO 950 PMMA A6 (MicroChem Corp.) spin-coated at 4000 rpm for 50 s on the samples, followed by electron beam evaporation and lift-off process and chemical etching. To remove redundant SOG, we dipped our sample in the buffered hydrofluoric acid (BHF) and rinsed it by purified water. We adjusted the dipping time by checking the etched condition via optical microscope. Typically, we repeated the procedure BHF etching of 10 s and checking the etched state until SOG is removed from the surface of the substrate. To introduce biaxial strain, electron beam (typically 80 kV of acceleration voltage and 2 nA of beam current) is irradiated on all the surface areas of the Ni films in Figure 1a,c and Figure 2a or on the two regions of the SOG film around the edges of the graphene flakes as shown in Figure 3c. To introduce in-plane isotropic

compressive strain, the sample is coated with the SOG film and heated on a hot plate with different baking temperatures at 190, 235, and 300 °C in the laboratory atmosphere.

Measurements of Raman Spectrum. Raman spectra are measured with the excitation laser wavelength of 532 nm, and the estimated diameter of the laser spot is 2−3 μm. The laser power is kept less than 1 mW to avoid damaging the graphene.

■ AUTHOR INFORMATION

Corresponding Author

*E-mail: shioya@meso.t.u-tokyo.ac.jp.

Notes

The authors declare no competing financial interest.

■ ACKNOWLEDGMENTS

We acknowledge Professor Y. Iwasa and Dr. K. Konishi for their technical support of Raman spectrum measurements. H. Shioya acknowledges financial support from GCOE for Phys. Sci. Frontier and from Project for Developing Innovation Systems, MEXT, Japan. M.Y. acknowledges financial support from Grant-in-Aid for Young Scientists A (No. 23684019) and MEXT KAKENHI "Science of Atomic Layers". S.T. acknowledges financial support from JST Strategic International Cooperative Programs (DFG-JST and EPSRC-JST).

■ REFERENCES

(1) Novoselov, K. S.; Geim, A. K.; Morozov, S. V.; Jiang, D.; Katsnelson, M. I.; Grigorieva, I. V.; Dubonos, S. V.; Firsov, A. A. Two-dimensional gas of massless Dirac fermions in graphene. *Nature* **2005**, *438*, 197−200.

(2) Zhang, Y.; Tan, Y.-W.; Stormer, H. L.; Kim, P. Experimental observation of the quantum Hall effect and Berry's phase in graphene. *Nature* **2005**, *438*, 201−204.

(3) Meric, I.; Han, M. Y.; Young, A. F.; Özyilmaz, B.; Kim, P.; Shepard, K. L. Current saturation in zero-bandgap, top-gated graphene field-effect transistors. *Nat. Nanotechnol.* **2008**, *3*, 654−659.

(4) Schwierz, F. Graphene transistors. *Nat. Nanotechnol.* **2010**, *5*, 487−496.

(5) Kim, K., Choi, J.-Y., Kim, T., Cho, S.-H., and Chung, H.-J., A role for graphene in silicon-based semiconductor devices. *Naure 479*, 338-344

(6) Otsuji, T.; Tombet, S. A. B.; Satou, A.; Fukidome, H.; Suemitsu, M.; Sano, E.; Popov, V.; Ryzhii, M.; Ryzhii, V. Graphene-based devices in terahertz science and technology. *J. Phys. D: Appl. Phys.* **2012**, *45*, 303001−303009.

(7) Craciun, M. F.; Russo, S.; Yamamoto, M.; Tarucha, S. Tuneable electronic properties in graphene. *Nano Today* **2011**, *6*, 42−60.

(8) Shioya, H.; Yamamoto, M.; Russo, S.; Craciun, M. F.; Tarucha, S. Gate tunable non-linear currents in bilayer graphene diodes. *Appl. Phys. Lett.* **2012**, *100*, 033113−033116.

(9) Guinea, F.; Katsnelson, M. I.; Geim, A. K. Energy gaps and a zero-field quantum Hall effect in graphene by strain engineering. *Nat. Phys.* **2009**, *6*, 30−33.

(10) Pereira, V. M.; Castro Neto, A. H. Tight-binding approach to uniaxial strain in graphene. *Phys. Rev. B* **2009**, *80*, 045401−045408.

(11) Ribeiro, R. M.; Pereira, V. M.; Peres, N. M. R.; Briddon, P. R.; Castro Neto, A. H. Strained graphene: tight-binding and density functional calculations. *New J. Phys.* **2009**, *11*, 115002−115012.

(12) Montambaux, G.; Piechon, F.; Fuchs, J.-N.; Goerbig, M. O. Merging of Dirac points in a two-dimensional crystal. *Phys. Rev. B* **2009**, *80*, 153412−153415.

(13) Pereira, V. M.; Castro Neto, A. H. Strain Engineering of Graphene's Electronic Structure. *Phys. Rev. Lett.* **2009**, *103*, 046801−046804.

(14) Levy, N.; Burke, S. A.; Meaker, K. L.; Panlasigui, M.; Zettl, A.; Guinea, F.; Castro Neto, A. H.; Crommie, M. F. Strain-Induced Pseudo-Magnetic Fields Greater Than 300 T in Graphene Nanobubbles. *Science* **2010**, *329*, 544−547.

(15) Lu, J.; Castro Neto, A. H.; Loh, K. P. Transforming moiré blisters into geometric graphene nano-bubbles. *Nat. Commun.* **2012**, DOI: 10. 1038/ncomms1818.

(16) Petrone, N.; Meric, I.; Hone, J.; Shepard, K. L. Graphene Field-Effect Transistors with Gigahertz-Frequency Power Gain on Flexible Substrates. *Nano Lett.* **2013**, *13*, 121−125.

(17) Kim, K. S.; Zhao, Y.; Jang, H.; Lee, S. Y.; Kim, J. M.; Kim, K. S.; Ahn, J.-H.; Kim, P.; Choi, J.-Y.; Hong, B. H. Large-scale pattern growth of graphene films for stretchable transparent electrodes. *Nature* **2009**, *457*, 706−710.

(18) Park, J. U.; Nam, S.; Lee, M.-S.; Lieber, C. M. Synthesis of monolithic graphene-graphite integrated electronics. *Nat. Mat.* **2012**, *11*, 120−125.

(19) Lee, S.-K.; Kim, B. J.; Jang, H.; Yoon, S. C.; Lee, C.; Hong, B. H.; Rogers, J. A.; Cho, J. H.; Ahn, J.-H. Stretchable Graphene Transistors with Printed Dielectrics and Gate Electrodes. *Nano Lett.* **2011**, *11*, 4642−4646.

(20) Lee, S.-K.; Jang, H. Y.; Jang, S.; Choi, E.; Hong, B. H.; Lee, J.; Park, S.; Ahn, J.-H. All Graphene-Based Thin Film Transistors on Flexible Plastic Substrates. *Nano Lett.* **2012**, *12*, 3472−3476.

(21) Kim, B. J.; Jang, H.; Lee, S.-K.; Hong, B. H.; Ahn, J.-H.; Cho, J. H. High-performance Flexible Graphene Field Effect Transistors with Ion Gel Gate Dielectrics. *Nano Lett.* **2010**, *10*, 3464−3466.

(22) Lu, C.-C.; Lin, Y.-C.; Yeh, C.-H.; Huang, J.-C.; Chiu, P.-W. High Mobility Flexible Graphene Field-Effect Transistors with Self-Healing Gate Dielectrics. *ACS Nano* **2012**, *6*, 4469−4474.

(23) Ni, Z. H.; Yu, T.; Lu, Y. H.; Wang, Y. Y.; Feng, Y. P.; Shen, Z. X. Uniaxial Strain on Graphene: Raman Spectroscopy Study and Band-Gap Opening. *ACS Nano* **2008**, *2*, 2301−2305.

(24) Mohiuddin, T. M. G.; Lombardo, A.; Nair, R. R.; Bonetti, A.; Savini, G.; Jalil, R.; Bonini, N.; Basko, D. M.; Galiotis, C.; Marzari, N.; Novoselov, K. S.; Geim, A. K.; Ferrari, A. C. Uniaxial strain in graphene by Raman spectroscopy: G peak splitting, Grüneisen parameters, and sample orientation. *Phys. Rev. B* **2009**, *79*, 205433−205440.

(25) Tsoukleri, G.; Parthenios, J.; Papagelis, K.; Jalil, R.; Ferrari, A. C.; Geim, A. K.; Novoselov, K. S.; Galiotis, C. Subjecting a Graphene Monolayer to Tension and Compression. *Small* **2009**, *5*, 2397−2402.

(26) Ferrari, A. C.; Meyer, J. C.; Scardaci, V.; Casiragi, C.; Lazzeri, M.; Mauri, F.; Piscanec, S.; Jiang, D.; Novoselov, K. S.; Roth, S.; Geim, A. K. Raman Spectrum of Graphene and Graphene Layers. *Phys. Rev. Lett.* **2006**, *97*, 187401−187404.

(27) Romero, J. D.; Kahn, M.; Fatemi, H.; Turlo, J. Outgassing behavior of spin-on-glass (SOG). *J. Mater. Res.* **1991**, *6*, 1996−2003.

(28) Liu, F.; Ming, P.; Li, J. *Ab initio* calculation of ideal strength and phonon instability of graphene under tension. *Phys. Rev. B* **2007**, *76*, 064120−064126.

(29) Lee, C.; Wei, X.; Kysar, J. W.; Hone, J. Measurement of the Elastic Properties and Intrinsic Strength of Monolayer Graphene. *Science* **2008**, *321*, 385−388.

(30) Guinea, F. Strain engineering in graphene. *Solid State Commun.* **2012**, *152*, 1437−1441.

(31) Lee, J. E.; Ahn, G.; Shim, J.; Lee, Y. S.; Ryu, S. Optical separation of mechanical strain from charge doping in graphene. *Nat. Commun.* **2012**, *3*, 1024.

(32) Shen, X.; Wang, H.; Yu, T. How do the electron beam writing and metal deposition affect the properties of graphene during device fabrication? *Nanoscale* **2013**, *5*, 3352−3358.

(33) Blake, P.; Hill, E. W.; Castro Neto, A. H.; Novoselov, K. S.; Jiang, D.; Yang, R.; Booth, T. J.; Geim, A. K. Making graphene visible. *Appl. Phys. Lett.* **2007**, *91*, 063124−063126.

(34) Koh, Y. K.; Bae, M.-H.; Cahill, D. G.; Pop, E. Reliably Counting Atomic Planes of Few-Layer Graphene ($n > 4$). *ACS Nano* **2011**, *5*, 269−274.